Supporting Information for "Two-photon microscopy with a double-wavelength metasurface objective lens"

Ehsan Arbabi,[†] Jiaqi Li,[‡] Romanus J. Hutchins,[§] Seyedeh Mahsa Kamali,[†] Amir Arbabi,[‖] Yu Horie,[†] Pol Van Dorpe,[‡] Viviana Gradinaru,[⊥] Daniel A. Wagenaar,[⊥] and Andrei Faraon[*,†]

†*T. J. Watson Laboratory of Applied Physics and Kavli Nanoscience Institute, California Institute of Technology, 1200 E. California Blvd., Pasadena, CA 91125, USA*

‡*IMEC, Kapeldreef 75, B-3001 Leuven, Belgium*

¶*Department of Physics and Astronomy, KU Leuven, Celestijnenlaan 200 D, B-3001 Leuven, Belgium*

§*Department of Physics and Astronomy, University of Missouri Columbia, MO 65211*

‖*Department of Electrical and Computer Engineering, University of Massachusetts Amherst, 151 Holdsworth Way, Amherst, MA 01003, USA*

⊥*Division of Biology and Biological Engineering, California Institute of Technology, Pasadena, CA 91125, USA*

E-mail: faraon@caltech.edu

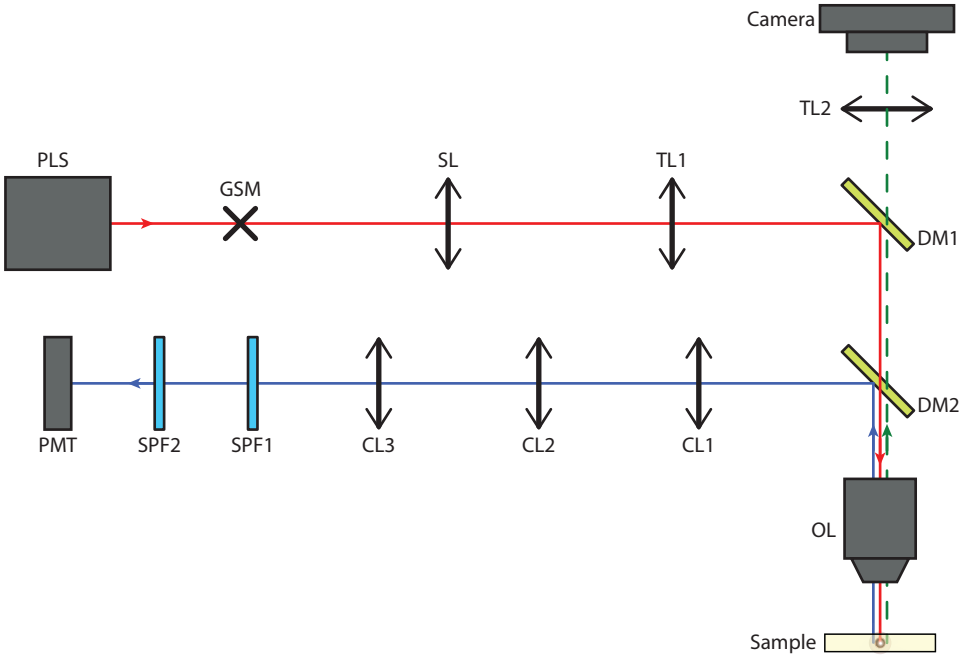

Figure S1: Schematics of the two-photon microscope. PLS: Pulsed laser source, Spectra-Physics InSight DS+. GSM: Galvanometer scanning mirror, Cambridge Tech 6215H. SL: Scan lens f=54 mm, Thorlabs LSM54-1050. TL1: Tube lens f=200 mm, Thorlabs ITL200. DM1: Dichroic mirror, reflects >805 nm, Thorlabs DMSP805L. DM2: Dichroic mirror, reflects 500–700 nm, Chroma T600/200dcrb. OL: Objective lens 20×/NA=0.5, Zeiss EC Epiplan-Neofluar (this objective is replaced by the DW-ML). CL1: Collection lens f=100 mm, Thorlabs AC508-100. CL2: Collection lens f=50 mm, Thorlabs LA1119. CL3: Collection lens f=30 mm, Thorlabs LA1085. SPF1: Short-pass filter <680 nm, Chroma ET680SP-2P8. SPF2: Short-pass filter <700 nm, Thorlabs FESH0700. PMT: Photomultiplier tube, Hamamatsu R3896. TL2: Tube lens f=75 mm, Thorlabs AC508-075. Camera: AmScope HD205-WU. The camera is only used to find the part of the sample that is of interest and bring it in focus.

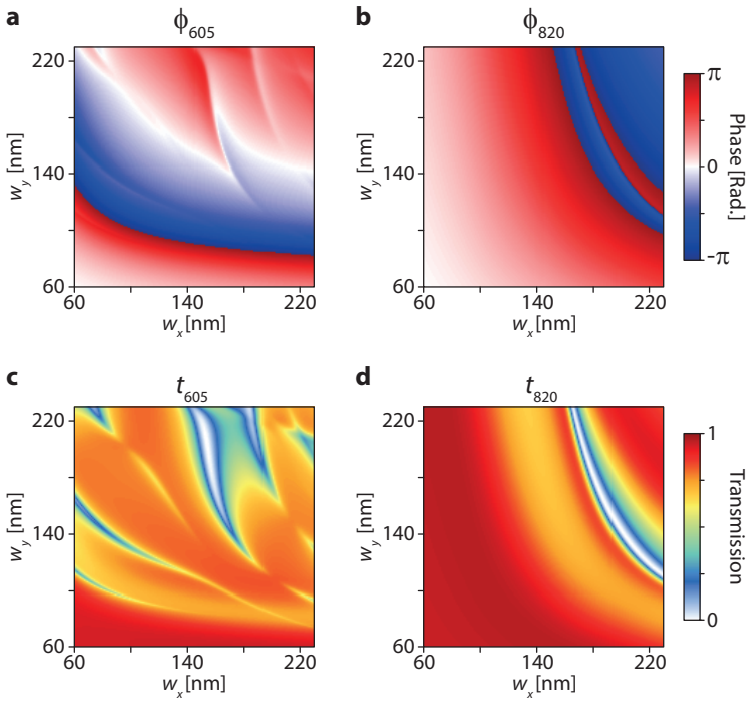

Figure S2: Simulated transmission phase and amplitude of a uniform array of nano-posts. (a) Simulated transmission phase of a uniform array of nano-posts at 605 nm, and (b) at 820 nm. (c) Simulated transmission amplitude of a uniform array of nano-posts at 605 nm, and (d) at 820 nm. Material loss contributes to the lower transmittance at 605 nm.

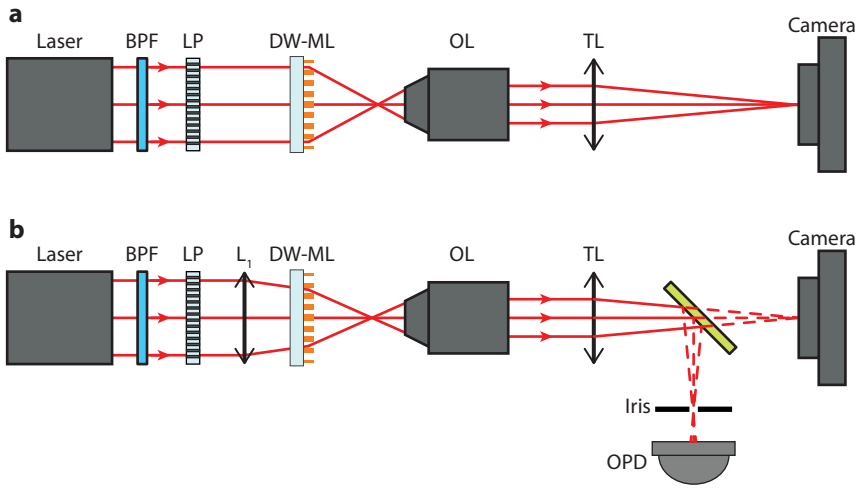

Figure S3: Schematics of the setups used to characterize the DW-ML. (a) Schematics of the setup used to capture the intensity distribution patterns of Fig. 3. Laser: ∼822-nm laser diode for measurements at 820 nm, and Fianium WhiteLase Micro supercontinuum laser for characterization at 605 nm. BPF: Band-pass filter with a center wavelength of ∼600 nm and FWHM of 10 nm (used only with the supercontinuum), Thorlabs FB600-10. LP: Linear polarizer, Thorlabs LPVIS100-MP2. OL: Objective lens 100×/NA=0.95, Olympus UMPlanFl. TL: Tube lens f=20 cm, Thorlabs AC254-200-B-ML. Camera: Photometric Coolsnap K4. (b) Schematic of the setup used to measure the focusing efficiency of the DW-ML. L_1: Lens.f=200 mm, Thorlabs AC254-200-B-ML. OPD: Optical power detector, Thorlabs PM100D with photodetector head Thorlabs S122C. L_1 is only used to partially focus light such that it has a ∼550-μm FWHM at the DW-ML plane. This way, more than 99% of the input light power passes through the lens. The iris diameter is 1.1 mm for 820 nm and 0.55 mm at 605 nm.

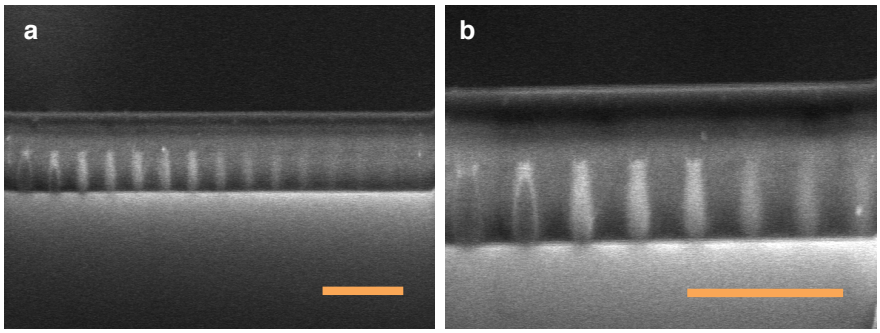

Figure S4: Cross-sectional scanning electron micrographs of metasurfaces cladded with an SU-8 polymer. (a) and (b) In both cases the metasurface layer is about 1 μm thick, and the SU-8 layer is $\sim$2 μm thick. It is seen that even in such an extreme case where the SU-8 layer is only twice as thick as the nano-posts, the final SU-8 layer surface is very smooth. Scale bars: 2 μm.

Section 1: Effects of chromatic dispersion on efficiency

In this section we first study the effect of the finite bandwidth of the light used to characterize the DW-ML at 605 nm. Second, we estimate the effect of the bandwidth of the pulsed laser on the excitation efficiency of the two-photon imaging. In both cases, we model the lens as a transmission mask with constant amplitude and phase over the bandwidth. This model results in an upper-bound for the efficiency as it only takes the diffractive chromatic dispersion into account, and overlooks the wavelength dependence of the nano-posts over the bandwidth of the pulse.

To estimate the apparent reduction in measured efficiency due to the finite bandwidth of the 600-nm source, we simulated the focusing of the DW-ML at 41 wavelengths (580 nm to 620 nm, at 1-nm separations). This bandwidth was chosen to completely cover the pass-band of the used filter. The simulation was performed through modeling the DW-ML as a complex transmission mask, and propagating the fields after the DW-ML using a plane-wave propagation code. To get the total intensity in the focal plane, the weighted intensities (using the transmission values of the bandpass filter) were added for all the wavelengths. The integral of this total intensity in a disk with a 5-μm diameter was divided to the total power before the DW-ML to achieve a $\sim$38$\%$ focusing efficiency. In addition, we calculated the efficiency at the center wavelength of 600 nm to be $\sim$63$\%$. Therefore, we estimated the experimental single wavelength focusing efficiency to be $\sim$45$\%$. As expected from our previous work, the experimental focusing efficiency at the shorter wavelength is more sensitive to fabrication errors.[1]

The excitation efficiency in the two-photon process is proportional to the intensity squared. To estimate the ratio of the peak intensity squared for the DW-ML and the conventional objective lens, we simulated both cases using the method explained above. We modeled the DW-ML by its transmission mask at 820 nm, and modeled the objective as a perfect aspherical phase mask. The pulsed laser has a $\lessapprox$120 fs width, and assuming a bandwidth-limited Gaussian pulse, we find that it has a $\gtrapprox$9 nm bandwidth. We calculated the electric field distribution in the focal plane for both the DW-ML and the conventional objective for all the wavelengths. Since the exact waveform of the pulse after passing through the setup is not known, we calculated the peak intensity ratio in two

extreme cases. First, we assumed that all different wavelengths add up in phase in the focal plane (corresponding to a case with the shortest possible pulse width and the largest peak-to-average power ratio). Second, we assumed that the pulse is completely broadened (with a peak-to-average power ratio of one). To model this, we added the simulated intensities of different wavelengths in the focal plane. With equal input powers for the DW-ML and the conventional objective, the peak intensity ratios in the two cases were $\sim$12.7 and $\sim$4.9, respectively. In reality, the ratio must be between these two values because the pulse reaching the focal point is broadened due to dispersion, yet it's not completely incoherent.

Using these pieces of data, we can estimate the contribution of different factors to the lower excitation-collection efficiency of the DW-ML compared to the conventional objective. As observed in Figs. 4b and 4c, the collected power with the DW-ML is about 0.06 of the collected power with the objective. In addition, the excitation laser power with the DW-ML is about 4.7 times larger than the objective. The collected power is proportional to the peak excitation intensity squared, and the collection efficiency. Therefore we can write

$$\frac{P_{\mathrm{OL}}^{\mathrm{Col}}}{P_{\mathrm{DW-ML}}^{\mathrm{Col}}} = \frac{\eta_{\mathrm{OL}}^{\mathrm{Col}}}{\eta_{\mathrm{DW-ML}}^{\mathrm{Col}}} \left(\frac{P_{\mathrm{OL}}^{\mathrm{Exc}}}{P_{\mathrm{DW-ML}}^{\mathrm{Exc}}} \frac{I_{\mathrm{OL}}^{p}}{I_{\mathrm{DW-ML}}^{p}}\right)^2 \tag{1}$$

where the subscripts determine the utilized lens (OL denoting the conventional objective lens), Col and Exc denote collection and excitation, and I^p is the peak intensity for the lenses calculated with equal excitation powers. Using this equation and the 22.5$\%$ collection efficiency of the DW-ML, we can estimate the $\frac{I_{\mathrm{OL}}^{p}}{I_{\mathrm{DW-ML}}^{p}}$ ratio to be $\sim$9.1. This ratio falls well within the 4.9-12.7 range that was calculated.

References

(1) Arbabi, E.; Arbabi, A.; Kamali, S. M.; Horie, Y.; Faraon, A. *Opt. Express* **2016**, *24*, 18468–18477.